SOIL SCIENCE ANNUAL
2023, 74(2), 169656

https://doi.org/10.37501/soilsa/169656

Mapping carbon dioxide (CO_2) emissions from peat subsidence using carbon parameters and InSAR observations in South Kalimantan, Indonesia

Noorkomala Sari[1], Noorlaila Hayati[2]*, Maulida A. Uzzulfa[2], Rahmat Arief[3], Trismono Candra Krisna[4]

[1] Universitas Lambung Mangkurat, Department of Agroecotechnology, Banjarbaru, South of Kalimantan, Indonesia 70714
[2] Institut Teknologi Sepuluh Nopember, Department of Geomatics Engineering, Surabaya, East of Java, Indonesia 60111
[3] National Research and Innovation Agency, Research Organization of Aeronautics and Space, Research Center of Remote Sensing, Indonesia 13710
[4] European Space Agency, European Space Research and Technology Centre, Netherlands, 2201

* Dr.-Ing Noorlaila Hayati, S.T., M.T., e-mail: noorlaila@geodesy.its.ac.id, ORCID iD: https://orcid.org/0000-0002-2703-111X

Received: 2022-10-19
Accepted: 2023-07-15
Published online: 2023-07-15
Associated editor: B. Glina

Keywords:

Carbon dioxide emission
Peatland
PS-InSAR
South Kalimantan
Subsidence

Abstract

Peatlands are recognized as one of the largest terrestrial carbon sinks and are pivotal in efforts to mitigate climate change. Given this, Indonesia has committed to managing its peatlands, which have been subjected to drainage, deforestation, fires, and conversion for development. As of 2015, the Center for Agricultural Land Resources has mapped 107,344 ha of peatlands in South Kalimantan Province. However, in 2019, forest fires destroyed 2,400 ha of land, leading to the decomposition of surface peat areas, land subsidence, and the release of carbon into the atmosphere as CO_2. This study aimed to quantify the widespread loss of peat carbon using the PS-InSAR (Persistent Scatterer Interferometric Synthetic Aperture Radar) technique. Specifically, 66 Sentinel 1 SAR images of SLC were used to map subsidence in the peatland area between January 2019 and January 2021. The carbon content and bulk density of peatland were then quantified to estimate CO_2 emission. The results obtained through the PS-InSAR technique showed that the highest level of peat subsidence was at –50 mm year^{-1} in the Landasan Ulin Sub–district of Banjarbaru Regency. Furthermore, subsidence was identified in 6,920.5 ha of peatland in the study area. Subsidence, peat area, and carbon content data from SAR images, optical images, and peat soils were gathered through field surveys and websites (GSOCMap and Zenodo) to estimate CO_2 emission. The estimated CO_2 emissions based on in–situ and website data were the highest at 0.29 t C ha^{-1} year^{-1} and 0.04 t C ha^{-1} year^{-1} in Beruntung Baru Sub-district, Banjar Regency, and Bumi Makmur Sub-district, Tanah Laut Regency, respectively.

1. Introduction

Peat is considered a type of soil made from decomposed organic material capable of absorbing (sequestering) and storing (sink) large amounts of carbon to prevent greenhouse gases from escaping into the earth's atmosphere, which can have an impact on climate change (Page et al., 2011) and peatland is type of wetland habitat that covered by peat soil. Indonesia has one of the world's largest peatland areas, with a total of 25 million ha, storing a large amount of carbon, estimated at 57 gigatonnes (Gt), or around 55% of the carbon in tropical peatland worldwide. (Kiely et al., 2021; Page et al., 2011; Dargie et al., 2017).

The total area of peatland in South Kalimantan was 107,344 ha in 2015 and decreased to 46,294 ha in 2019 by BBSDLP (2019), as cited in Anda et al. (2021). Persistent environmental change, such as drainage and forest clearing, threatens stability, making them susceptible to fire (Page et al., 2002). Forest fire is one of the main causes of peat destruction / degradation. This was demonstrated by widespread fires in the peat forest in Central Kalimantan, Borneo, during the 1997 El Niño event. Furthermore, Page et al. (2002) calculated that every 0.0007 ha burned peatland area results in 0.19–0.23 Gt carbon released to the atmosphere.

Various problems that cause peatland subsidence and its relation to the release of carbon into the atmosphere as CO_2 are oxidation, shrinkage, and compaction triggered by fires and large or small-scale drainage developments around plantations (Saputra, 2019). According to data from the Regional Disaster Management Agency of South Kalimantan, the area of forest and land fires in 2019 reached 7,800 ha and 2,400 ha of peatland (Susanto et al., 2020). Due to deforestation, forest degradation, and burning, the stored CO_2 can return to the atmosphere, contributing to climate change and global warming (Waqar et al., 2020).

Mapping CO_2 emissions on peatland using remote sensing methods is necessary to determine the amount of CO_2 released. Remote sensing techniques may help upscale and understand

the surface height change rate over time (Zhou et al., 2016). The SAR (Synthetic Aperture Radar) satellite sensor can measure the elevation of the earth surface (Dyatmika et al., 2018) and allows observations of the surface day or night in all weather conditions from aerial and space platforms (Dahlal, 2011). Several SAR sensors operate simultaneously at different frequencies, providing potentially useful data for monitoring surface movement over tropical peatland (Umarhadi et al., 2021). Therefore, this study used the advanced InSAR approach, PS-InSAR (Persistent Scatterer Interferometric Synthetic Aperture Radar), which adopts many SAR image pairs to obtain the value of peatland subsidence to the cm-mm level. The technique overcomes the problems in the InSAR technique related to temporal and geometric decorrelation (Prasetyo and Subiyanto, 2014).

Zhou et al. (2016) used the InSAR technique with SAR images to monitor peatland subsidence. Meanwhile, CO_2 emissions were estimated based on the subsidence, the peat volume loss, and the C loss rates in the period of 2006–2010 (multi-temporal). The results showed deficiencies in decorrelation caused by the long observation period. This is because more data were needed with close temporal distances to increase accuracy. Another study in Central Kalimantan (Nuthammachot et al., 2019) estimated the burnt area in the ex-Mega Rice Project (MRP) and calculated carbon emissions from peat fires using TerraSAR-X imagery for April 2010. In addition, study to calculate carbon emission estimates was carried out on burned peatland in Siak District, Riau Province (Hafni et al., 2018). The data were obtained from Landsat-8 imagery based on the NBR vegetation index, and the biomass was measured using the allometric method. Therefore, the PS-InSAR technique was used for monitoring peatland subsidence from January 2019 to 2021 to estimate CO_2 emissions in some parts of Banjar Regency, Tanah Laut Regency, and Banjarbaru City, South Kalimantan. The selection of study locations was based on specific criteria, including the detection of peatland subsidence in South Kalimantan using the InSAR technique and land cover classification.

This study estimated carbon dioxide emissions using a mathematical model based on several factors, including peat subsidence rate, peatland area, carbon content, and peat bulk density. Furthermore, it determines the approximate area of peatland cover in the sampling area to estimate the changes in peat volume detected as subsidence by the PS-InSAR approach. The carbon loss will be assessed based on the integration of in-situ measurements and InSAR remote sensing techniques. The estimation of CO_2 emission is calculated from the peat subsidence rate, carbon content, and peat bulk density equation. This calculation is conducted independently to compare web source and field data sets, resulting in two scenarios.

2. Materials and methods

2.1 Study area

The study area encompassed Banjar Regency, Tanah Laut Regency, and Banjarbaru City, focusing on six specific sub-districts, namely Gambut, Beruntung Baru, Bumi Makmur, Liang Anggang, Landasan Ulin, and Cempaka. These sub-districts were located between latitudes –3°32’1” and –3°22’20” and longitudes 144°49’12” E and 144°35’12” E. The selection of soil sample area in peatland was based on PS-inSAR analysis and field validation, resulted on 17 observation points, as shown in Fig. 1.

2.2. Data processing of SAR using PS-InSAR time series

The first dataset was peatland subsidence, obtained from the processing of Sentinel-1. This was conducted using the PS-InSAR time series technique with slowly decorrelating filtered

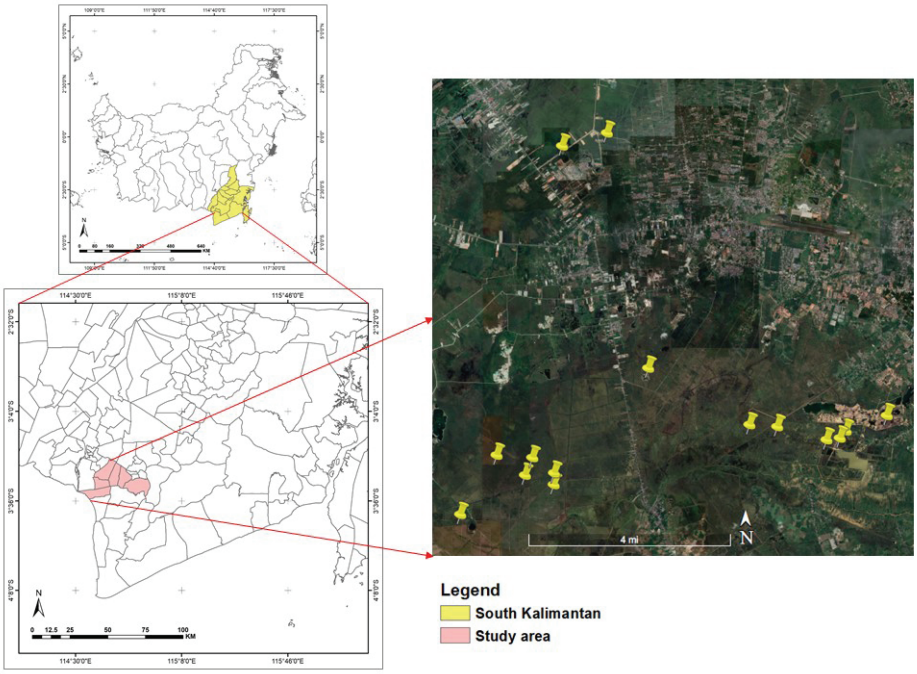

Fig. 1. Location of the study area, the yellow pointers indicate the observation points

phase (SDFP) pixels (Hooper et al., 2008) from January 2019 to 2021, according to the previous study by Hayati et al. (2022). It was converted into raster data using the surface gridding method in GMT. Furthermore, the second dataset was Landsat-8 surface reflectance images obtained from Google Earth Engine. It was used to classify land cover objects based on the study of Wijedasa et al. (2012), which consists of 5 classes, namely bare earth/urban areas, agriculture, disturbed peatland, prime peatland, and open water. Subsequently, Landsat-8 images were displayed in false color composite bands (654) and (753) as the basis for making samples (Putra et al., 2017). A supervised land cover classification method was then performed with the Classification and Regression Trees (CART) algorithm. The accuracy test was carried out on the results of land cover classification by making samples using comparative data, such as field surveys of peat areas, high-resolution satellite images on Google Earth Engine (GEE) and Google Earth Pro, as well as land cover maps of South Kalimantan 2020 from the Ministry of Environment and Forestry of Indonesia. Furthermore, the classified land cover was reclassified, which separated disturbed and prime peat classes to obtain subsidence data based on 17 observation points.

According to Hayati et al. (2022), the last data were obtained from fields and websites. The data included carbon content, bulk density, peat thickness, and organic carbon released as CO_2. In situ methods used a peat sampler, 5–9 extension rods, and one set of handles to make up the Eijkelkamp peat drill, which was used to sample peat soil in assessing carbon content (C-org) and peat depth. Meanwhile, the gravimetric approach was used in the lab to calculate the bulk Density (BD) obtained using a ring sampler. The Loss on Ignition method was used to determine the carbon content of the soil sample. The entire organic content was burned at a temperature of 550°C for six hours. The burned organic material vaporized, leaving behind inorganic compounds such as soil clay, dust particles, and fine sand. The weight of the organic matter lost during the combustion of the oven-dried soil samples was determined. In contrast, the carbon content and bulk density data in 2019 and 2017 were obtained from the GSOCmap website and OpenLandMap.org (Hengl, 2018). The equation used to calculate the values of soil density, and carbon content was provided by Agus et al. (2011).

$$BD = \frac{M_S}{V} \quad \text{Equation 1}$$

$$BD = (M_S + M_C) - \frac{M_C}{(\pi \times r^2 \times t)} \quad \text{Equation 2}$$

$$C_v = BD \times \left(\frac{C_{org}}{100}\right) \quad \text{Equation 3}$$

Description:
BD – bulk density, M_s – the dry weight of soil, M_c – sample ring weight, V – sample ring volume, r – ring radius, t – ring height, C_v – carbon content per soil volume, C_{org} – organic carbon

Carbon content data obtained from the GSOCMap website were available in a different unit, tons $ha^{-1,}$ while in this study, tons m^{-3} (carbon content per soil volume) was used. Therefore, to change the units, a conversion was performed, which involved calculations using a thickness of peat and organic carbon from field data with the following equation (Agus et al., 2011):

$$C_V = \frac{Carbon\ content\ per\ soil\ layer\ (\text{ton ha}^{-1})}{Soil\ volume\ per\ layer\ (\text{m}^3\ \text{ha}^{-1})} \quad \text{Equation 4}$$

$$Soil\ volume\ per\ layer = Peat\ thickness\ (\text{m}) \times 10.000 \quad \text{Equation 5}$$

A correlation analysis examined the relationship between the carbon content and bulk density data. In the event of a low correlation, the two variables were treated as independent inputs in the CO_2 emission equation, creating two distinct scenarios based on data obtained from the field and website.

2.3. Carbon dioxide emission calculation

Dariah (2011) asserted that the source of greenhouse gas emissions is very high due to the drainage of peatland, about 13.1 t C ha^{-1} y^{-1} (Annisa and Nursyamsi, 2017). Additionally, the correlation between CO_2 emissions and the groundwater table depth was found to be positive, with higher CO_2 emissions occurring at greater depths. In many instances, land use boundaries are reflected in subsidence patterns due to differences in drainage depths between adjacent areas. Peat properties, such as depth, degree of decomposition, and mineral content, also contribute to the variability of subsidence rates. Furthermore, subsidence rates can be impacted by warming temperatures resulting from climate and land use change (Hoyt et al., 2020). According to Othman et al. (2011), temperature variations in tropical regions play a minor role in affecting the groundwater table. However, CO_2 emissions are strongly dependent on this factor. Lowering the groundwater table by draining the area results in peat subsidence, which is responsible for decreasing peat depth and increasing bulk density (Othman et al., 2011). The relationship between monitoring CO_2 and groundwater depth has been discussed by Hooijer et al. (2009) to calculate gas emissions using the following equation.

$$CO_2\ emission = 3{,}67 \times Area \times WT \times C1m\ (ty^{-1}) \times P \quad \text{Equation 6}$$

Description:

$$WT = \frac{peat\ subsiden\ cerate\ (\text{cmy}^{-1})}{XO} \quad \text{Equation 7}$$

$$C1m = carbon\ content \times peat\ bulk\ density \times XO \quad \text{Equation 8}$$

The value of XO is eliminated through Equations 7 and 8, hence Equation 6 will be,

$$CO_2\ emission = 3{,}67 \times area \times peat\ subsiden\ cerate\ (cmy^{-1}) \times \times carbon\ content \times peat\ bulk\ density \times P \quad \text{Equation 9}$$

Description:
3.67 – conversion factor carbon to carbon dioxide, area – dry or burnt peat area (ha), WT – average change in groundwater depth (cm y^{-1} or m y^{-1}), C1m – loss of carbon at an average groundwater depth of 1 m (t C^{-1} ha^{-1} y^{-1}), XO – coefficient of groundwater level change and the rate of groundwater subsidence (assumed 0.04~0.1 according to previous study by Wosten et al. (1997) and Wosten and Ritzema (2001)), P – the percentage of carbon released as carbon dioxide.

3. Result

3.1. Land cover classification and Peatland subsidence

The area of 5 land cover classes is presented in Table 1, and an accuracy test was performed by taking 38 polygon samples. Furthermore, the accuracy assessment of the classification result was calculated using the confusion matrix method and overall accuracy. In this test, an accuracy value of 85.3% was obtained, as shown in Table 2. The land cover can be seen in the overall accuracy value. Meanwhile, the disturbed and prime peat classes were overlaid with subsidence data based on 17 observation points, as shown in Fig. 4.

Fig. 2 depicts four observation points, namely TS25 and TS26, as the lowest subsidence levels, as well as TS29 and TS30, as the highest subsidence levels, with values of –94 mm in January 2021 and –107 mm in October 2020, respectively. Moreover, Table 3 and Fig. 3 present the data sets on the average subsidence rate (mm year–1) from January 2019 to 2021, demonstrating subsidence levels at 17 observation points ranging from –50 to –5 mm year^{-1}.

According to Fig. 3, subsidence was observed in all 17 observation points. However, the extent was relatively lower in the northern part of the study area than in the southern part. The four observation points in the northern part, namely TS11, TS12, TS25, and TS26, exhibited the lowest subsidence values. Fig. 4 presents a map that outlines the subsidence levels of both disturbed and prime peatland based on the 17 observation points, covering an area of 6,920 ha.

Table 1
Land Cover Area Classification Results

Land cover class	Area (ha)
Bare earth/urban areas	4,811
Agriculture	14,849
Disturbed peatland	9,741
Prime peatland	5,884
Open water	339
Total	35,624

Table 2
Confusion matrix and overall accuracy

		Samples					Total	Correct pixels
		1	2	3	4	5		
Class image	1	377	6	15	0	0	398	2709
	2	40	1827	75	89	1	2032	
	3	1	47	145	18	0	211	
	4	0	99	63	312	0	474	
	5	0	0	0	13	48	61	
Total		418	1979	298	432	49	3176	
Overall accuracy		85,296						

where: 1 – bare earth/urban areas, 2 – agriculture, 3 – disturbed peatland, 4 – prime peatland, 5 – open water

Table 3
Average subsidence rate from January 2019 to January 2021

Point	Average rate (mm year^{-1})	Point	Average rate (mm year^{-1})
TS1	–29	TS15	–20
TS2	–25	TS16	–24
TS3	–28	TS17	–38
TS4	–24	TS18	–32
TS5	–39	TS25	–7
TS6	–29	TS26	–5
TS11	–10	TS29	–47
TS12	–19	TS30	–50
TS13	–23		

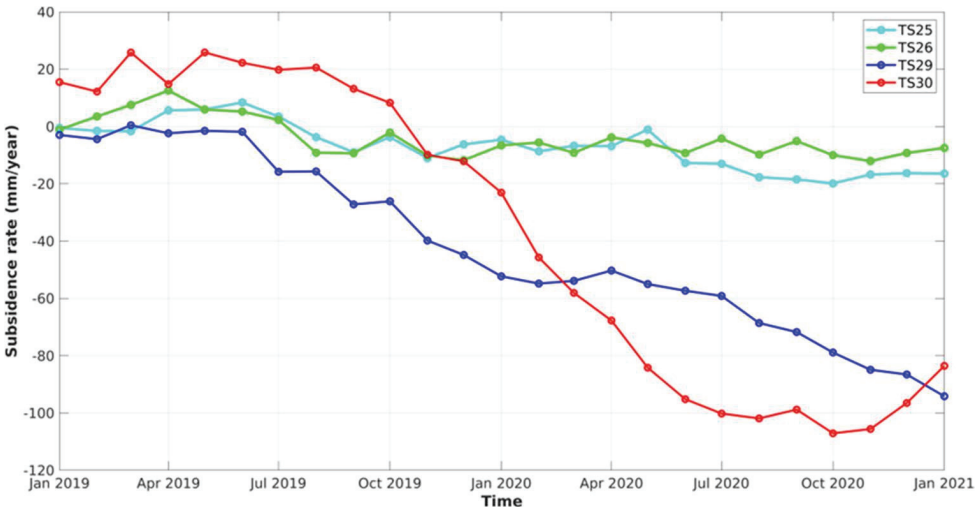

Fig. 2. Time series graph of the subsidence rate from January 2019 to January 2021. TS25 (114.7035°, –3.4187°) and TS26 (114.6907°, –3.4224°) showing the stable area in the northern part while, based on the descending trend lines, TS29 (114.7522°, –3.5024°) and TS30 (114.7442°, –3.5018°) indicating siginificant subsidence occured in the southern part of study area.

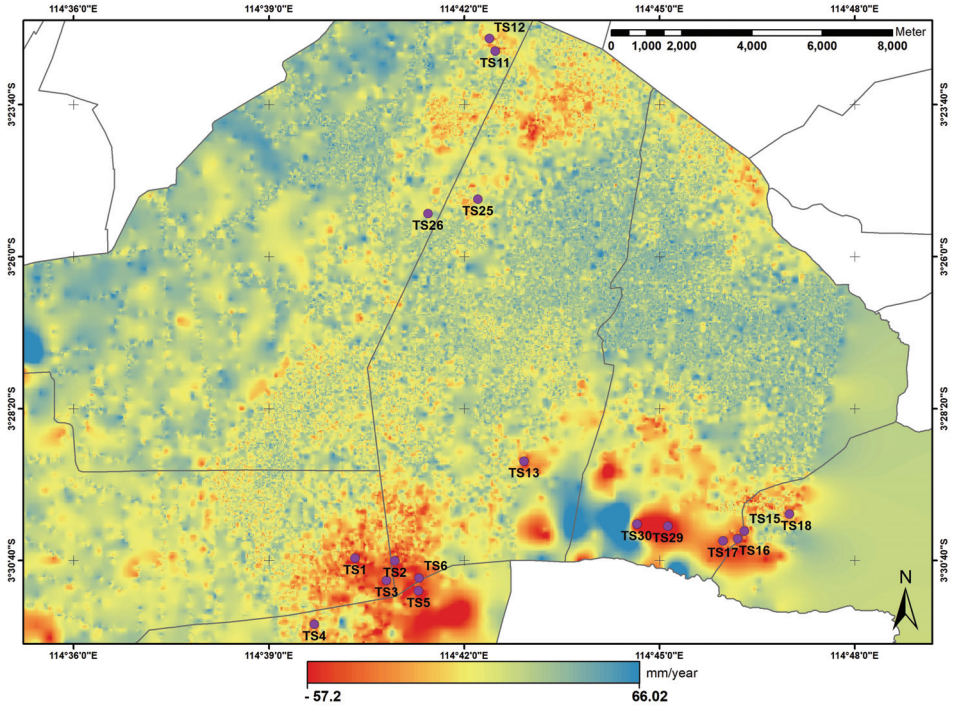

Fig. 3. Map of average subsidence rate (mm year^{-1}) from January 2019 to January 2021

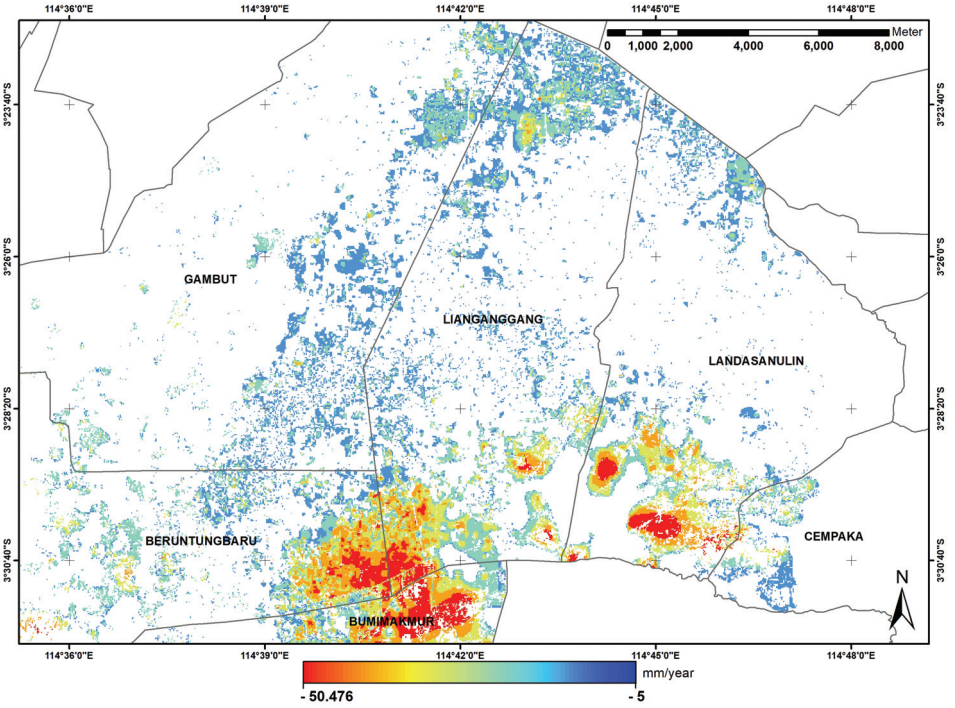

Fig. 4. Map of peatland subsidence with the detected peatland areas obtained by the false colour composite image classification. The subsidence area has been intersecting with the classification of land cover for disturbed and prime peatland generated from Landsat-8 surface reflectance.

3.2. Carbon content and bulk density data

There are discrepancies between the year of data acquisition from the field, which was 2021, and from the website, including data from 2017 and 2019. Therefore, substantial differences existed in the values of the two data sources, as indicated in Table 4. According to the field data sources, TS3 exhibited the highest bulk density and carbon content values, measuring 0.71 and 0.39 t m^{-3}, respectively. Based on the website data sources, TS29 and TS4 exhibited the highest soil density and carbon content values, measuring 0.11 t m^{-3} and 0.57 t m^{-3}.

3.3. Estimation result of CO_2 emission

The calculation of CO_2 emissions in the study area was based on Equation 9, using a P value or percentage of carbon released as CO_2 of 100%. Therefore, all the carbon released into the atmosphere is in the form of CO_2. The area parameter used in the calculation was the spatial resolution of all the raster data previously resampled to 30 x 30 m, equivalent to 0.09 ha. This was because one observation point (TS) corresponds to one pixel, which is equivalent to the spatial resolution of the raster data. Table 5 and Fig. 5 present the monthly CO_2 emission rate from January 2019 to 2021.

Table 4
Carbon content and bulk density values

Points	Field data source		Website data source*	
	Bulk density (t m^{-3})	Carbon content (t m^{-3})	Bulk density (t m^{-3})	Carbon content (t m^{-3})
TS1	0.60	0.32	0.11	0.05
TS2	0.69	0.38	0.05	0.06
TS3	0.71	0.39	0.04	0.06
TS4	0.66	0.33	0.09	0.57
TS5	0.45	0.24	0.07	0.07
TS6	0.57	0.31	0.04	0.08
TS11	0.23	0.10	0.05	0.00
TS12	0.17	0.08	0.05	0.00
TS13	0.50	0.26	0.04	0.06
TS15	0.25	0.13	0.07	0.05
TS16	0.27	0.14	0.09	0.07
TS17	0.25	0.13	0.08	0.07
TS18	0.34	0.18	0.08	0.08
TS25	0.47	0.23	0.06	0.07
TS26	0.16	0.08	0.08	0.03
TS29	0.30	0.16	0.11	0.04
TS30	0.32	0.17	0.10	0.05

*source GSOCMap and OpenLandMap

Table 5
Estimated of average CO_2 emission rate from January 2019 to January 2021

Point	Estimated CO_2 emission rate from field data (t C ha^{-1} $year^{-1}$)	Estimated CO_2 emission rate from website data (t C ha^{-1} $year^{-1}$)
TS1	0.19	0.01
TS2	0.26	0.00
TS3	0.29	0.00
TS4	0.21	0.04
TS5	0.14	0.01
TS6	0.17	0.00
TS11	0.01	0.00
TS12	0.01	0.00
TS13	0.09	0.00
TS15	0.03	0.00
TS16	0.03	0.00
TS17	0.04	0.01
TS18	0.06	0.01
TS25	0.05	0.00
TS26	0.00	0.00
TS29	0.08	0.01
TS30	0.09	0.01
Total	1.75	0.10

The time series of the estimated rate of CO_2 emissions in Table 5 (field data source) can be illustrated in the following graph.

The time series of the estimated rate of CO_2 emissions in Table 5 (website data source) can be illustrated in the following graph.

Fig. 5 shows 4 observation points, namely TS2, TS3, TS12, and TS26. From field data sources, TS2 and TS3 were the points with the highest CO_2 emission values in December 2020 at 0.54 and 0.65 t C ha^{-1}, while TS12 and TS26 had the lowest. The reason of low CO_2 emission value is that TS2 and TS3 were located in the prime peatlands and belonged to a conservation area as seen on the documentation picture showing a natural environment. Regarding the result of in-situ observation on those points, the C organic still maintained as a high value (indicated in Table 4) and C loss was considered low. Furthermore, Fig. 6 from the website data source consists of TS4 and TS29, with the highest CO_2 emission values in January 2021 of 0.09 and 0.02 t C ha^{-1}, while TS11 and TS12 had the lowest.

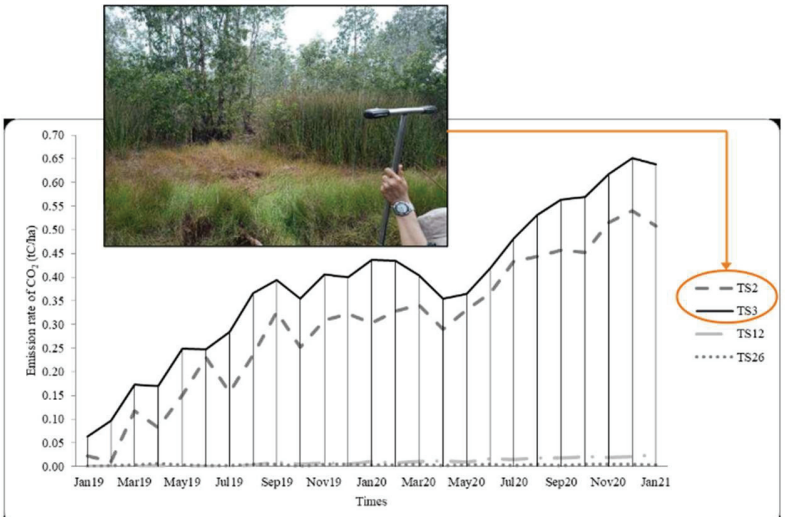

Fig. 5. Time series graph of the CO_2 emission rate (field data source) from January 2019 to January 2021

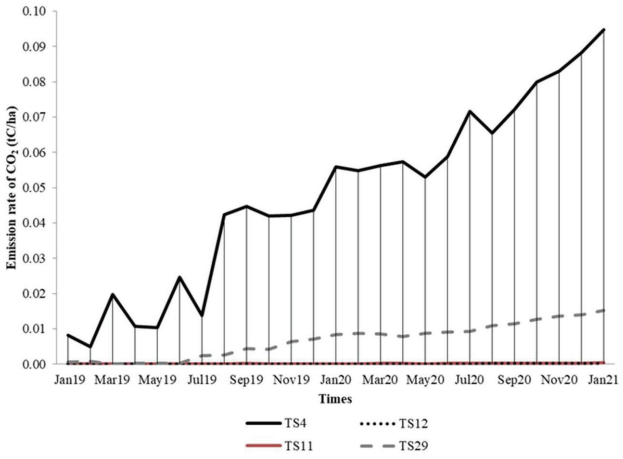

Fig. 6. Time series graph of the CO_2 emission rate (website data source) from January 2019 to January 2021

The presented data on the average CO_2 emission rate from January 2019 to January 2021, which was calculated using both field and website data sources, are shown in Figs. 7 and 8. Fig. 7 shows that the emission rate varies from 0 to 0.36 t C ha^{-1} year^{-1}, with the highest value recorded in TS3, located in the southern part of the study area, specifically in Beruntung Baru Sub-district, with a value of 0.29 t C ha^{-1} year^{-1}. Similarly, in Fig. 11, the average rate ranges from 0 to 0.05 t C ha^{-1} year^{-1}, with the highest value recorded in TS4, located in the southern part of the study area, specifically in Bumi Makmur Sub-district, with a value of 0.04 t C ha^{-1} year^{-1}.

The southern and northern parts of the study area are characterized by observation points with higher and lowest CO_2 emissions. Additionally, Table 5 highlights that TS3 has the highest CO_2 emissions level from the field data sources. This result is consistent with the largest carbon content recorded in TS3 and the relatively high subsidence rate of –28 mm year^{-1}, indicating that large subsidence occurs when peat soil contains

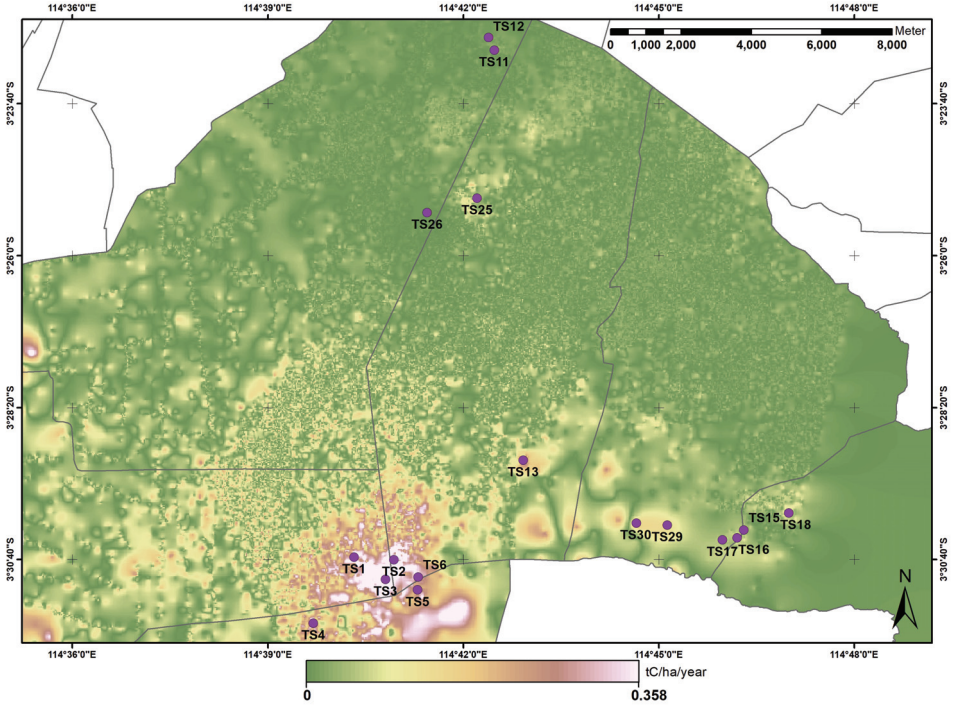

Fig. 7. Average CO_2 emission rate (field data sources) from January 2019 to January 2021

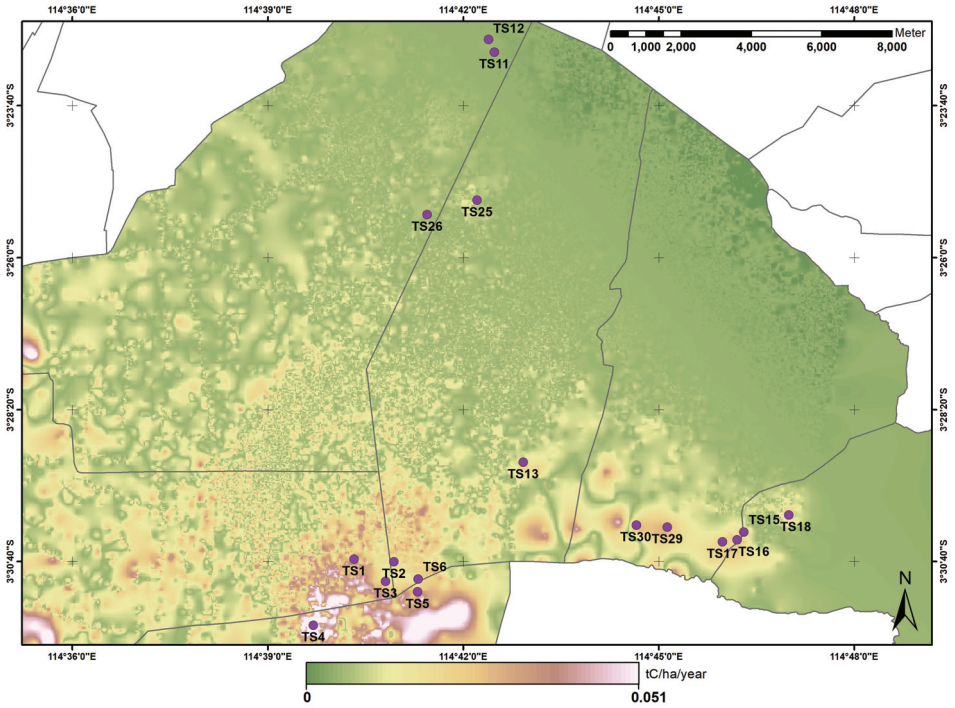

Fig. 8. Average CO_2 emission rate (website data sources: GSOCMap and OpenLandMap) from January 2019 to January 2021

a large amount of carbon, resulting in the release of a considerable amount into the atmosphere.

3.4. Correlation of field and website data parameters

Table 6 illustrates the correlation coefficient (r) calculation for field and website data sources. The correlation coefficient aims to establish a close relationship between two or more variables.

Table 6
Parameter correlation of field data and website

Coefficient correlation (r)		Website data*		
		Bulk density	Carbon content	CO_2 emission
Field data	Bulk density	–0.27	0.42	0.39
	Carbon content	–0.28	0.37	0.35
	CO_2 emission	–0.32	0.08	0.17

*source GSOCMap and OpenLandMap

4. Discussion

4.1. Land cover classification and Peatland subsidence

Notably, the highest value was recorded at TS30, located in the southern part of the study area, Landasan Ulin sub-district, which is primarily utilized for agricultural activity, such as paddy fields, and consequently receives the lowest precipitation levels. The observed subsidence rates and peatland degradation could be attributed to changes in water availability, as previously reported by Zhou et al. (2019), where precipitation has been identified as a determining factor in subsidence levels.

The low-high rate of subsidence is influenced by plantation forestry. Alshammmari et al. (2018) reported that these areas dominated by stability or uplift are far from drainage lines and feature a peatland pool system. Plantation can decrease the water content of underlying peat and cause subsidence. Furthermore, groundwater drainage in the study area may alter the hydraulic properties of deep peat and induce continued subsidence (Regan et al., 2019). The peatland observed in Riau, Indonesia, showed that the reduction in the groundwater table caused by drainage canals has significantly impacted peat subsidence. This impact will become even more critical when the area is burned for land use change, as it creates an impermeable layer on peat surfaces that limits the water infiltration rate, thereby exacerbating the situation (Basuki et al., 2021).

Subsidence rates may vary depending on regional peat characteristics such as peat depth, degree of decomposition, and mineral content (Hoyt et al., 2020). Temperature increases may also have an impact on subsidence rates due to changes in land use and climate. Further parameters of land use and climate change will be studied in further research.

4.2. Carbon content and bulk density data

The high carbon content value can be attributed to the reason that the area had been disturbed and converted into an oil palm plantation. Vicharnakorn et al. (2014) stated that soil microbial activities in a fibrous root system increased, generating an ideal environment rich in organic carbon. Meanwhile, the thickness of peat affects the amount of carbon content stored in the soil. Dariah (2011) reported that the thicker the peat, the greater the carbon reserves. This applies to the parameter of carbon content per layer/depth (t ha^{-1}). However, this study used the parameter of carbon content per soil volume (t m^{-3}) as described in Equation 4, which is inversely proportional to the thickness of peat.

Based on Equation 3, the value of carbon content is directly proportional to the bulk density. Therefore, the bulk density and carbon content values are directly proportional, as shown in Table 4 on the field data sources. This relationship does not apply to the website data source due to the difference in the acquisition time of the two data sets. Therefore, the two data sets are not directly comparable. Potential causes for slowed subsidence, as stated by Hoyt et al. (2020), include (1) a change in peat properties when preferential decomposition of labile organic matter leaves behind a more stable peat matrix, (2) drainage depths could decrease over time when canals are not maintained, (3) in some cases, such as the area in TS3, all peat may have decomposed, exposing the underlying mineral soil and lowering averages rates for old plantations.

4.3. Estimation result of CO_2 emission

Reported by Zhou et al., (2016) peatland was deforested and drained in Southeast Asia. These processes allow the surface peat to degrade and release carbon dioxide into the atmosphere, which results in lowering both their capacity for future soil C storage and their strength as a present C store. However, there are obstacles to related quantitative CO_2 emission estimation. It can be challenging to monitor peatland surface height changes using field–based surveys over the vast areas that were frequently drained in the past, therefore measurements are more likely to represent a limited area and serve as a snapshot in time.

The southern and northern parts of the study area are characterized by observation points with higher and lowest CO_2 emissions. Additionally, Table 5 highlights that TS3 has the highest CO_2 emissions level from the field data sources. This result is consistent with the largest carbon content recorded in TS3 and the relatively high subsidence rate of –28 mm $year^{-1}$, indicating that large subsidence occurs when peat soil contains a large amount of carbon, resulting in the release of a considerable amount into the atmosphere.

4.4. Correlation of field and website data parameters

It is observed that the CO_2 emission variable from the website data displays a positive correlation with the emissions field data. As highlighted in Table 5, the results from the two data sources differ considerably. A hypothesis test was performed us-

ing a critical value to determine the significance of the correlation coefficient. Furthermore, a two-tail test was utilized since the correlation coefficient has both negative and positive values. At a significance level of a = 0.05, the critical value for the number of paired observations (n = 17) is 0.48. In evaluating the Pearson's correlation coefficients (r) of all three variables against the positive and negative critical values, the null hypothesis is accepted, indicating that no correlation exists. Consequently, the observed r values in a sample of n=17 observations are not significantly different from random and cannot be employed as the line for prediction.

5. Conclusion

Based on the results, it can be concluded that the calculation of the estimated CO_2 emissions involves the integration of subsidence data, area of peatland, and data on carbon content and bulk density of peat soil. The results showed that the highest subsidence was –50 mm year^{-1} at TS30 in Landasan Ulin sub-district, Banjarbaru City. The area of peat using the spatial resolution of raster data for all parameters was 0.09 ha, with a subsidence value of 6,920 ha. The data on carbon content and bulk density were collected from field and website sources. Furthermore, the field data was used as validation, but both had a low correlation. The highest value of peatland CO_2 emission in the study area from January 2019 to 2021 was 0.29 t C ha^{-1} year^{-1} in TS3, Beruntung Baru Sub-district, Banjar Regency. Meanwhile, The highest value of peatland CO_2 emission from website data in the study area was 0.04 t C ha^{-1} year^{-1}, in TS4, Bumi Makmur Sub-district, Tanah Laut Regency.

Acknowledgment

The project was funded by JASTIP-NET (Japan-ASEAN Science, Technology and Innovation Platform) in 2021: Partnership and Networking (WP1) and the Directorate of Research and Community Service (DRPM), Institut Teknologi Sepuluh Nopember. The authors gratefully acknowledge Copernicus Open Access Hub for the access free to the Sentinel-1 SAR and Global Land Cover Facility (GLCF) for the DEM SRTM.

References

Agus, F., Hairiah, K., Mulyani, A., World Agroforestry Centre (ICRAF), 2011. Pengukuran cadangan karbon tanah gambut. Balai Besar Penelitian dan Pengembangan Sumberdaya Lahan Pertanian, Bogor, Indonesia, Universitas Brawijaya, Malang, Indonesia.

Annisa, W., Nursyamsi, D. 2017. Potensi Emisi Karbon di Lahan Gambut Tropis. https://polbangtan-bogor.ac.id

Alshammari, L., Large, D.J., Boyd, D.S., Sowter, A., Anderson, R., Andersen, R., Marsh, S., 2018. Long-Term Peatland Condition Assessment via Surface Motion Monitoring Using the ISBAS DInSAR Technique over the Flow Country, Scotland. Remote Sensing 10(7), 1103. https://doi.org/10.3390/rs10071103

Anda, M., Ritung, S., Suryani, E., Sukarman, Hikmat, M., Yatno, E., Mulyani, A., Subandiono, R.E., Suratman, Husnain. 2021. Revisiting tropical peatlands in Indonesia: Semi-detailed mapping, extent and depth distribution assessment. Geoderma, 402, 115235. https://doi.org/https://doi.org/10.1016/j.geoderma.2021.115235

Basuki, I., Budiman, A., Netzer, M., Safitri, R., Maulana, R., Nusirhan, T.S.E., Syamsir, & Bernal, B., 2021. Dynamic of groundwater table, peat subsidence and carbon emission impacted from deforestation in tropical peatland, Riau, Indonesia. IOP Conference Series: Earth and Environmental Science 648(1), 12029. https://doi.org/10.1088/1755-1315/648/1/012029

Susanto, D., Sanusi, Widyanti, R., 2020. Implementasi Kebijakan Restorasi Gambut di Kalimantan Selatan dari Persfektif Komunikasi Kebijakan (Studi Kasus di Kecamatan Candi Laras Utara Kabupaten Tapin). Doctoral dissertation, Universitas Islam Kalimantan MAB. https://eprints.uniska-bjm.ac.id/id/eprint/401

Dahlal, B., 2011. The use of interferometric spaceborne radar and GIS to measure ground subsidence in peat soils in Indonesia. University of Leicester. Thesis. https://hdl.handle.net/2381/10254

Dariah, A., Susanti, E., Agus, F., 2011. Simpanan karbon dan emisi CO_2 di lahan gambut. Pengelolaan lahan gambut berkelanjutan. Balai Penelitian Tanah. p. 56–72.

Dargie, G.C., Lewis, S.L., Lawson, I.T., Mitchard, E.T., Page, S.E., Bocko, Y.E., Ifo, S.A., 2017. Age, extent and carbon storage of the central Congo Basin peatland complex. Nature 542(7639), 86–90.

Dyatmika, H.S., Arief, R., Sudiana, D., Ali, S., Maulana, R., 2018. Modifikasi Digital Elevation Model (DEM) Citra Resolusi Tinggi Menggunakan Fusi Interferometri SAR dan StereoSAR Berbasis Faktor Pembobotan. 15(2), 10. https://dx.doi.org/10.30536/j.pjpdcd.2018.v15.a3063

Directorate of Peatland Degradation Control Republic of Indonesia. 2021. Corrective Action on Peatland Protection and Management in Indonesia-Toward Sustainable Peatland Management 2019–2020. Ministry of Environment and Forestry Republic of Indonesia. Retrieved from https://pkgppkl.menlhk.go.id

Hafni, D., Syaufina, L., Puspaningsih, N., Prasasti, I., 2018. Estimation of carbon emission from peatland fires using Landsat-8 OLI imagery in Siak District, Riau Province. IOP Conf. Ser.: Earth and Environmental Science 149, 012040. https://doi.org/10.1088/1755-1315/149/1/012040

Hayati, N., Sari, N., Arief, R., Uzzulfa, M.A., 2022. Parameters To Estimate CO_2 Emission in Peatland Area Based on Carbon Content and Subsidence Rate from Sar Interferometry, Int. Arch. Photogramm. Remote Sens. Spatial Inf. Sci., XLIII-B3-2022, 277–284, https://doi.org/10.5194/isprs-archives-XLIII-B3-2022-277-2022

Hengl, T., 2018. Soil bulk density (fine earth) 10 x kg / m-cubic at 6 standard depths (0, 10, 30, 60, 100 and 200 cm) at 250 m resolution [Map]. https://zenodo.org/record/2525665#.YoOQl9NBzDf

Hooper, A., 2008, A multi-temporal InSAR method incorporating both persistent scatterer and small baseline approaches, Geophysical Research Letters 35, L16302, doi:10.1029/2008GL034654

Hooijer, A., Page, S., Canadell, J.G., Silvius, M., Kwadijk, J., Wösten, H., Jauhiainen, J., 2009. Current and future CO_2 emissions from drained peatlands in Southeast Asia [Preprint]. Biogeochemistry: Greenhouse Gases. https://doi.org/10.5194/bgd-6-7207-2009

Hoyt, A.M., Chaussard, E., Seppalainen, S.S. et al. Widespread subsidence and carbon emissions across Southeast Asian peatlands. 2020. Nature Geoscience 13, 435–440. https://doi.org/10.1038/s41561-020-0575-4

Kiely, L., Spracklen, D.V., Arnold, S.R., Papargyropoulou, E., Conibear, L., Wiedinmyer, C., Knote, C., Adrianto, H.A., 2021. Assessing costs of Indonesian fires and the benefits of restoring peatland. Nature Communications 12(1), 7044. https://doi.org/10.1038/s41467-021-27353-x

Nuthammachot, N., Phairuang, W., Stratoulias, D., 2019. Estimation of Carbon Emission in The Ex-Mega Rice Project, Indonesia Based on SAR Satellite Images. Applied Ecology and Environmental Research 17(2), 2489–2499. https://doi.org/10.15666/aeer/1702_24892499

Othman, H.A.S.N.O.L., Mohammed, A.T., Darus, F.M., Harun, M.H., Zambri, M.P., 2011. Best management practices for oil palm cultivation on peat: ground water-table maintenance in relation to peat subsidence and estimation of CO_2 emissions at Sessang, Sarawak. Journal of Oil Palm Research 23(2), 1078–1086.

Page, S., Siegert, F., Rieley, J., Boehm, H., Jaya, A., Limin, S., 2002. The amount of carbon released from peat and forest fires in Indonesia during 1997. Nature 420, 61–65. https://doi.org/10.1038/nature01131

Page, S.E., Rieley, J.O., Banks, C.J. 2011. Global and regional importance of the tropical peatland carbon pool. Global Change Biology 17(2), 798–818.

Putra, A., Sutikno, S., Rinaldi, 2017. Identifikasi Lahan Gambut Menggunakan Citra Satelit Landsat 8 OLI TIRS Berbasis Sistem Informasi Geografis (SIG) Studi Kasus Pulau Tebing Tinggi. 4(2), 11. Diss. Riau University.

Prasetyo, Y., Subiyanto, S., 2014. Studi Penurunan Muka Tanah (Land Subsidence) Menggunakan Metode Permanent Scatterer Interferometric Synthetic Aperture Radar (PS-InSAR) di Kawasan Kota Cimahi–Jawa Barat. Teknik 35(2), 78–85. https://doi.org/10.14710/teknik.v35i2.7184

Regan, S., Flynn, R., Gill, L., Naughton, O., Johnston, P., 2019. Impacts of groundwater drainage on peatland subsidence and its ecological implications on an Atlantic raised bog. Water Resources Research 55, 6153–6168. https://doi.org/10.1029/2019WR024937

Saputra, E., 2019. Beyond fires and deforestation: Tackling land subsidence in peatland areas, a case study from Riau, Indonesia. Land 8(5), 76. https://doi.org/10.3390/land8050076

Umarhadi, D.A., Avtar, R., Widyatmanti, W., Johnson, B.A., Yunus, A.P., Khedher, K.M., Singh, G., 2021. Use of multifrequency (C-band and L-band) SAR data to monitor peat subsidence based on time-series SBAS InSAR technique. Land Degradation and Development 32(16), 4779–4794. https://doi.org/10.1002/ldr.4061

Vicharnakorn, P., Shrestha, R.P., Nagai, M., Salam, A.P., Kiratiprayoon, S. Carbon Stock Assessment Using Remote Sensing and Forest Inventory Data in Savannakhet, Lao PDR. 2014. Remote Sensing 6(6), 5452–5479. https://doi.org/10.3390/rs6065452

Waqar, M.M., Sukmawati, R., Ji, Y., Sri Sumantyo, J.T., 2020. Tropical Peat-Land Forest Biomass Estimation Using Polarimetric Parameters Extracted from RadarSAT-2 Images. Land 9, 193. https://doi.org/10.3390/land9060193

Wijedasa, L.S., Sloan, S., Michelakis, D.G., Clements, G.R., 2012. Overcoming Limitations with Landsat Imagery for Mapping of Peat Swamp Forests in Sundaland. 2012. Remote Sensing 4(9), 2595–2618. https://doi.org/10.3390/rs4092595

Wosten, J., Ismail, A., Van Wijk, A., 1997. Peat subsidence and its practical implications: A case study in Malaysia. Geoderma 78(1), 25—36. https://doi.org/10.1016/S0016-7061(97)00013-X

Wosten, J., Ritzema, H., 2001. Land and water management options for peatland development in Sarawak, Malaysia. International Peat Jounal, 59–66.

Zhou, Z., Li, Z., Waldron, S., Tanaka, A., 2016. Monitoring peat subsidence and carbon emission in Indonesia peatlands using InSAR time series. 2016. IEEE International Geoscience and Remote Sensing Symposium (IGARSS), 6797–6798. https://doi.org/10.1109/IGARSS.2016.7730774

Zhou, Z., Li, Z., Waldron, S., Tanaka, A., 2019. InSAR time series analysis of L-band data for understanding tropical peatland degradation and restoration. Remote Sensing 11(21), 2592. https://doi.org/10.3390/rs11212592